JOC The Journal of Organic Chemistry

Article

pubs.acs.org/joc

1′,5′-Anhydro-L-*ribo*-hexitol Adenine Nucleic Acids (α-L-HNA-A): Synthesis and Chiral Selection Properties in the Mirror Image World

Daniele D'Alonzo,*[,†] Mathy Froeyen,[‡] Guy Schepers,[‡] Giovanni Di Fabio,[†] Arthur Van Aerschot,[‡] Piet Herdewijn,[‡] Giovanni Palumbo,[†] and Annalisa Guaragna[†]

[†]Dipartimento di Scienze Chimiche, Università degli Studi di Napoli Federico II, via Cintia 21, 80126 Napoli, Italy

[‡]Laboratory for Medicinal Chemistry, Rega Institute for Medical Research, KU Leuven, Minderbroedersstraat 10, 3000 Leuven, Belgium

Supporting Information

ABSTRACT: The synthesis and a preliminary investigation of the base pairing properties of (6′ → 4′)-linked 1′,5′-anhydro-L-*ribo*-hexitol nucleic acids (α-L-HNA) have herein been reported through the study of a model oligoadenylate system in the mirror image world. Despite its considerable preorganization due to the rigidity of the "all equatorial" pyranyl sugar backbone, α-L-HNA represents a versatile informational biopolymer, in view of its capability to cross-communicate with natural and unnatural complements in both enantiomeric forms. This seems the result of an inherent flexibility of the oligonucleotide system, as witnessed by the singular formation of iso- and heterochiral associations composed of regular, enantiomorphic helical structures. The peculiar properties of α-L-HNA (and most generally of the α-HNA system) provide new elements in our understanding of the structural prerequisites ruling the stereoselectivity of the hybridization processes of nucleic acids.

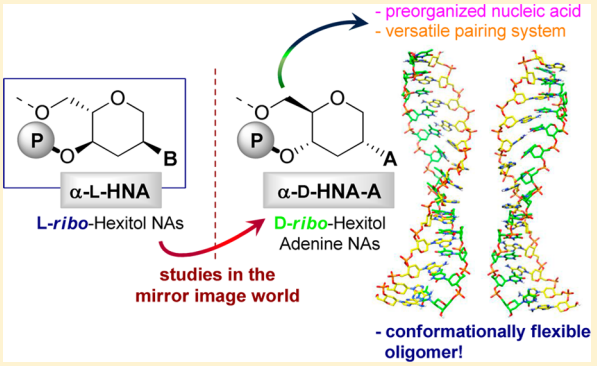

INTRODUCTION

Over the last few decades, the propensity for base pairing—through Watson−Crick or any other recognition mode—has been established not to be restricted only to natural nucleic acids, but has been found to be rather widespread among alternative genetic polymers recruited from the structural neighborhood of DNA and RNA.[1,2] Particularly, oligonucleotide systems involving replacement of the native (deoxy)-ribofuranose core with either preorganized[3,4] or flexible[5,6] sugar units have often been demonstrated to possess superior self- and cross-pairing properties, thereby representing excellent candidates for biomedical purposes,[3,5] inspiring etiological investigations on life's origin[6,7] and opening up a new world for information storage, propagation, and evolution.[8] In this area, the family of stereoisomeric six-membered oligonucleotides composed of (6′ → 4′)-linked 1′,5′-anhydrohexitol nucleotides (HNA, Figure 1) has been identified as one of the most powerful and versatile classes of synthetic informational polymers discovered to date.[4] The earliest and most prominent member of this family is the oligonucleotide system with D-*arabino* configuration (β-D-HNA).[9,10] β-D-HNA has been demonstrated to possess a remarkable hybridization aptitude toward natural complements, acting as an A-type (RNA) mimic[2b] (Figure 1). Besides its manifest potential as a therapeutic agent (e.g., as antisense,[11] *si*RNA,[12] and aptamer probes[13]) and as a diagnostic tool,[14] the β-D-HNA system was well suited for templated synthesis, under both chemical[15] and enzymatic[16] conditions, even in vivo,[17] acting both as substrate for oligonucleotide synthesis and as template for reverse transcription.[18] Very recently, HNA-based enzymes (HNAzymes) have been synthesized and found capable to display RNA endonuclease activity.[19]

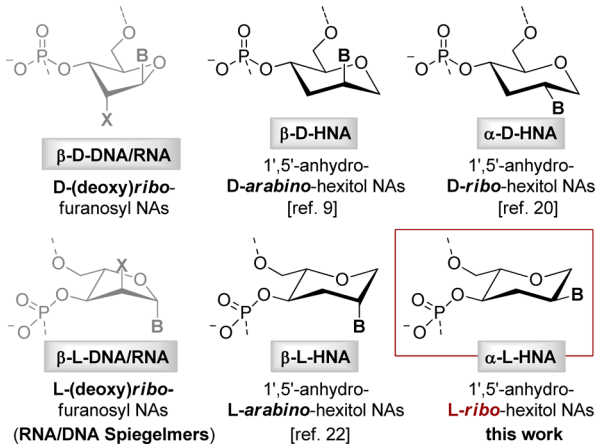

Figure 1. Stereoisomeric oligonucleotides belonging to the HNA family.

Received: February 20, 2015
Published: April 8, 2015

DOI: 10.1021/acs.joc.5b00406
J. Org. Chem. 2015, 80, 5014−5022

Among β-D-HNA stereoisomers, its C2′ epimer (i.e., the hexitol nucleic acid having D-*ribo* configuration: α-D-HNA) also was demonstrated to form stable complexes with RNA, with its conformationally constrained analogues (β-HNA, CNA) and other alternative oligonucleotide systems (e.g., β-homoDNA) having the same sugar chirality.[20] Different from β-D-HNA, its optical antipode (1′,5′-anhydro-L-*arabino*-hexitol nucleic acids: β-L-HNA), designed to potentially act as a conformationally constrained oligonucleotide spiegelmer,[21] was not able to pair with natural complements.[22] On the other hand, it exhibited the singular property of pairing with β-HNA complements (among other artificial oligonucleotide systems) belonging to both (same and opposite) senses of chirality.[22] This peculiarity, so far restricted only to a limited number of six-membered nucleic acids,[23−25] has inspired etiology-oriented studies aimed at elucidating the existing relationship between sugar structure and chiral selection properties of nucleic acids.[25−27] Intrigued by the remarkable hybridization potential of the HNA family, we have herein widened the repertoire of HNA stereoisomers by exploring the base pairing properties of a novel oligonucleotide system composed of (6′ → 4′)-linked 1′,5′-anhydro-L-*ribo*-hexitol nucleotides (α-L-HNA; Figure 1). Our interest in α-L-HNA comes from its potential pairing versatility, lying in its capability to reproduce the structure of two oligonucleotide systems having opposite hybridization profiles. Indeed, because of the "all-equatorial" pyranyl sugar unit in the backbone, α-L-HNA is expected to hold structural and conformational similarities with the six-membered oligonucleotide system composed of (6′ → 4′)-linked β-L-*erythro*-hexopyranosyl nucleotides (β-L-homoDNA; Figure 2a). The

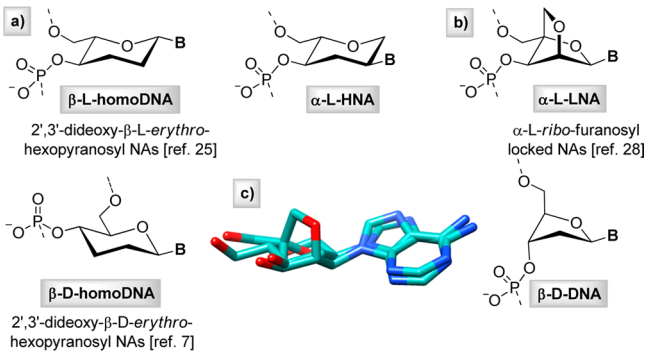

Figure 2. (a and b) Backbone similarities among α-L-HNA, β-D-*erythro*-hexopyranosyl nucleic acids (β-D-homoDNA), and α-L-*ribo*-pentofuranosyl locked nucleic acids (α-L-HNA). (c) Superimposition of the energy-minimized structures (Hyperchem 8.0, MP3 algorithm) of adenine nucleosides of α-L-HNA and α-L-LNA.

latter and its more prominent D-enantiomer (β-D-homoDNA)[7] belong to a class of preorganized pairing systems (pyranosyl nucleic acids) characterized by excellent self- and cross-communication properties, albeit unable to transfer information to natural nucleic acids. On the other hand, α-L-HNA is conceived to act as a mimic of the locked nucleic acid with α-L-*ribo* configuration, i.e. α-L-LNA (Figure 2b). The latter is a highly efficient DNA- and RNA-targeting pairing system, in turn acting as a DNA mimic because of the close resemblance of its dioxabicyclo[2.2.1]heptane skeleton to the bioactive C2′-*endo* sugar ring pucker of natural deoxynucleotides.[28] The structural analogy between the sugar units of α-L-LNA and α-L-HNA is preliminarily suggested by the energy-minimized structures of the corresponding adenine nucleosides, aligned to show a fairly close three-dimensional fit (Figure 2c).

The synthesis and an early evaluation of the hybridization properties of α-L-HNA [(oligo)adenylates being preliminarily considered] to natural and unnatural complements were carried out through studies in the mirror image world.[29] Accordingly, in place of a direct evaluation of the hybridization potential of α-L-HNA by annealing experiments with D-oligonucleotides (e.g., D-DNA and D-RNA), we instead conceived to perform hybridization studies of its mirror image (α-D-HNA) with complementary sequences of L-oligonucleotides (e.g., commercially available L-DNA and L-RNA). Exploiting the principles of chirality and enantiomeric recognition of nucleic acids, this evaluation was expected to indirectly provide information on the hybridization properties of our target α-L-HNA system.

RESULTS AND DISCUSSION

Nucleoside synthesis. An expeditious route to the 1′,5′-anhydro-D-*ribo*-hexitol nucleoside **13** to be used as building block for oligonucleotide synthesis was carried out as depicted in Schemes 1 and 2. Compared to previous synthetic

Scheme 1. Synthesis of D-*ribo*-Hexitol Nucleosides. Part I: Preparation of Alcohol Intermediate 5

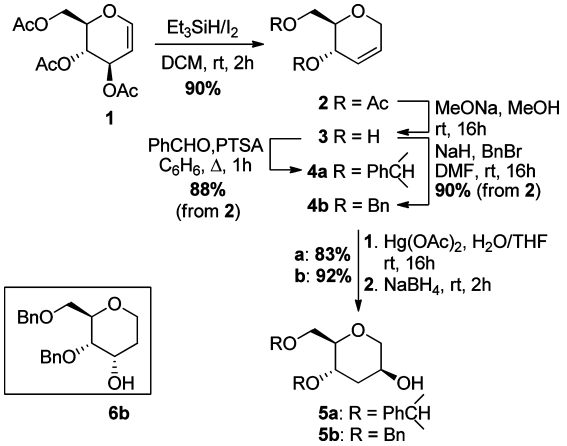

approaches devised to the same end,[20,30] an alternative path was herein envisioned starting from commercially available 3,4,6-tri-*O*-acetyl-D-glucal (**1**). Rearrangement of **1** under modified[31] Ferrier conditions (Et_3SiH/I_2) yielded the corresponding 2,3-unsaturated sugar **2** (90%). Then, after protective group replacement [MeONa, then NaH/BnBr (90% over two steps) or PhCHO/PTSA (88% over two steps)], regio- and stereoselective double bond hydration of **4a−b** was achieved using classical oxymercuriation/demercuriation conditions [$Hg(OAc)_2$, then $H_2O/NaBH_4$] (Scheme 1). In line with previous data,[32] treatment of **4a** with $Hg(OAc)_2$ in a H_2O/THF mixture followed by *one-pot* addition of $NaBH_4$ to the reaction mixture yielded alcohol **5a** as the only isomer in a good 83% yield. Under the same conditions, use of *bis*-benzyl ether **4b** as starting material provided **5b** with an even better yield (92%), although traces of the regioisomer **6b** were also detected (5%).[33]

Tosylation (TsCl/Py) of **5a−b** (Scheme 2) led to tosyl esters **7a−b** (88−90%), which were then subjected to coupling reaction with unprotected adenine (A/NaH). Disappointingly, deoxyadenosine analogue **8a** was obtained only in 25% yield, while undesired olefins **4a** and **9a** were recovered as the main

DOI: 10.1021/acs.joc.5b00406
J. Org. Chem. 2015, 80, 5014−5022

Scheme 2. Synthesis of D-*ribo*-Hexitol Nucleosides. Part II: Preparation of Amidite 13

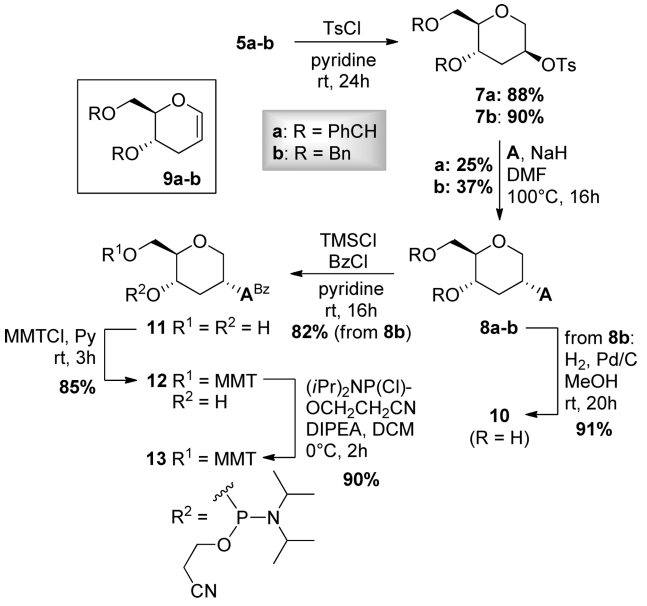

products. The same reaction, conducted starting from **7b**, provided nucleoside **8b** with a slightly better yield (37%). Standard nucleoside chemistry involving benzyl groups removal of **8b** (Pd/C, H_2, 91%), chemoselective *N*-benzoylation of **10** (TMSCl/BzCl), regioselective 6′-*O*-monomethoxytritylation of **11** (MMTCl, 85%), and 4′-*O*-phosphitylation of **12** [$(i\text{-Pr})_2$NP(Cl)OCH_2CH_2CN/DIPEA, 90%] eventually gave phosphoramidite monomer **13** to be used for incorporation studies.

Hybridization studies in the mirror image world. Assembly of oligonucleotides went flawless, and analogous yields were obtained in comparison to the assembly of natural oligonucleotides and to fully modified L-DNA and L-RNA sequences. Typically, yields of minimal 15 up to 50 OD_{260} were obtained for all 1 to 1.5 μmol scale reactions (hand-filled columns) following anion exchange HPLC purification and desalting.

To preliminarily assess the pairing potential of α-L-HNA toward natural complements, thermal denaturation studies in the mirror image world between α-D-HNA-(D-$^{\alpha}\mathbf{A}^{H}$)-containing oligomers and L-DNA/L-RNA complements were carried out (Tables 1 and 2). In all cases, compared to unmodified *ds*-L-DNA, *ds*-L-RNA, or L-DNA:L-RNA duplexes, incorporation of D-hexitol nucleotides led to a reduced thermal stability of the corresponding complexes (Table 1). Duplex destabilization was especially apparent with DNA: incorporation of a single D-hexitol nucleotide into a *ds*-L-DNA duplex led to a drop in the T_m value of the corresponding complex of about 14 °C (Table 1, entries 1−2). Further insertions of contiguous D-hexitol nucleotides caused a similar or even greater destabilization of the system (entries 3−7). Internal incorporations of D-hexitol nucleotides into L-DNA:L-RNA and *ds*-L-RNA duplexes analogously produced highly unstable complexes (entries 9 and 12). On the other hand, incorporations at the side positions provided a minor destabilization of the duplexes (entries 10 and 13). As an example, four contiguous α-D-HNA building blocks inserted into a L-DNA:L-RNA duplex did not alter the thermodynamic stability of the latter (ΔT_m: −0.7 °C) (entries 8 and 10). A similar incorporation into a *ds*-L-RNA duplex instead produced a less stable hybrid (ΔT_m: −8.2 °C; entries 11 and 13), although the latter still displayed a regular sigmoidal denaturation curve. Considering the data in the mirror image world, the apparent discrepancy of the data of Table 1 could be likely overcome hypothesizing that α-L-HNA holds a propensity for pairing with D-RNA, even though not acting as a D-DNA mimic. Accordingly, internal incorporations

Table 1. Thermal Stability Studies of *ds*-L-DNA, *ds*-L-RNA, and L-DNA:L-RNA Duplexes Containing One or More D-*ribo*-Hexitol Nucleotides[a]

5′-L-d(T_6**X**T_6)-3′				
Entry	**X**	Complement	T_m [°C]	ΔT_m [°C]
1	L-dA	L-DNA	29.6[b]	
2	D-$^{\alpha}$A^{H}	L-DNA	15.7[b]	−13.9
5′-L-d(T_5**X**$_3T_5$)-3′				
Entry	**X**	Complement	T_m [°C]	ΔT_m [°C]
3	L-dA	L-DNA	30.3[b]	
4	D-$^{\alpha}$A^{H}	L-DNA	ND[b,c]	
5′-L-d(**X**$_3$**Y**T_3A**T**ZT_2)-3′						
Entry	**X**	**Y**	**Z**	Complement	T_m [°C]	ΔT_m [°C]
5	L-dA	L-dA	L-dA	L-DNA	38.0	
6	L-dA	D-$^{\alpha}$A^{H}	D-$^{\alpha}$A^{H}	L-DNA	14.3	−23.7
7	D-$^{\alpha}$A^{H}	D-$^{\alpha}$A^{H}	L-dA	L-DNA	17.2	−20.8
8	L-dA	L-dA	L-dA	L-RNA	22.5	
9	L-dA	D-$^{\alpha}$A^{H}	D-$^{\alpha}$A^{H}	L-RNA	ND[c]	
10	D-$^{\alpha}$A^{H}	D-$^{\alpha}$A^{H}	L-dA	L-RNA	21.8	−0.7
5′-L-(**X**$_3$**Y**U_3A**U**ZU_2)-3′						
Entry	**X**	**Y**	**Z**	Complement	T_m [°C]	ΔT_m [°C]
11	L-rA	L-rA	L-rA	L-RNA	34.7	
12	L-rA	D-$^{\alpha}$A^{H}	D-$^{\alpha}$A^{H}	L-RNA	10.0	−24.7
13	D-$^{\alpha}$A^{H}	D-$^{\alpha}$A^{H}	L-rA	L-RNA	26.5	−8.2

[a]Melting points were determined at 260 nm in 1 M NaCl, 20 mM KH_2PO_4 (pH 7.5), 0.1 mM EDTA (unless otherwise specified). [b]Experiments conducted in 0.1 M NaCl buffer. [c]ND: no regular transition detected.

Table 2. Thermal Stability Studies of Iso- and Heterochiral Complexes Containing a Fully Modified α-D-HNA Strand [D-($^{\alpha}\mathbf{A}^{H}$)$_{13}$][a]

Entry	Oligonucleotide[b]	Complement	T_m [°C]
1	α-D-HNA	none	41.7
2	α-D-HNA	L-DNA	41.7[c,d]
3	α-D-HNA	D-DNA	41.8[c,d]
4	L-DNA	L-DNA	47.0
5	L-DNA	L-RNA	29.0
6	L-RNA	L-DNA	40.5
7	L-RNA	L-RNA	35.0
8	α-D-HNA	L-RNA	20.0
9	α-D-HNA	D-RNA	40.3[e]
10	α-D-HNA	β-D-HNA	67.0[c,f]
11	α-D-HNA	β-L-HNA	69.0[f]
12	α-D-HNA	β-D-homoDNA	50.1[f]
13	α-D-HNA	β-L-homoDNA	58.9[f]

[a]Melting points were determined at 260 nm in 1 M NaCl, 20 mM KH_2PO_4 (pH 7.5), 0.1 mM EDTA (unless otherwise specified). [b]13-mer oligoadenylates were used in all cases. [c]Referred to an $^{\alpha}\mathbf{A}^{H}$:$^{\alpha}\mathbf{A}^{H}$ association. [d]The formation of hairpin structures was excluded by concentration-dependent thermal denaturation studies (see the Supporting Information, Figure S7). [e]Taken from ref 20. [f]Experiments conducted in 0.1 M NaCl buffer.

DOI: 10.1021/acs.joc.5b00406
J. Org. Chem. 2015, 80, 5014−5022

of single modified nucleotides would strongly perturb the regularity of the natural A/B-type duplexes, while side incorporations of even several hexitol nucleotides would be better tolerated.

Along this line, annealing experiments of the fully modified α-D-HNA sequence D-$(^{\alpha}\mathbf{A}^{H})_{13}$ with DNA/RNA complements in both enantiomeric forms were performed (Table 2). α-D-HNA did not pair with D- or L-DNA, both at 0.1 and 1 M NaCl; the formation of an intermolecular $^{\alpha}\mathbf{A}^{H}$:$^{\alpha}\mathbf{A}^{H}$ association (T_m 41.7 °C) was instead detected in both cases (entries 1−3). On the other hand, regular sigmoidal curves were clearly observed after annealing of D-$(^{\alpha}\mathbf{A}^{H})_{13}$ with D- and L-RNA complements (entries 8−9). Looking at the mirror image world, it is worth mentioning that, to the best of our knowledge, this represents the first case of an oligonucleotide system with an L-hexose derivative in the backbone displaying hybridization with natural complements. However, the thermodynamic stability of the complex was very low (T_m 20 °C) and lower than that of the corresponding unmodified DNA:RNA duplex (T_m 29 °C; entry 5). Unexpected but not unprecedented,[25] no trace of the thermodynamically more stable $^{\alpha}\mathbf{A}^{H}$:$^{\alpha}\mathbf{A}^{H}$ complex (T_m 41.8 °C) was detected in this case.[34]

A comparative CD analysis of iso- and heterochiral hybrids was also carried out (Figure 3). The differences between the

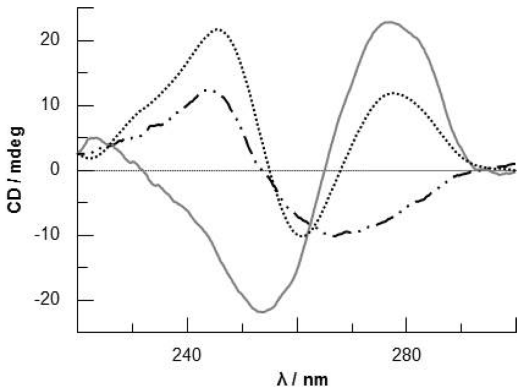

Figure 3. CD spectra of *ds*-α-D-HNA [*ds*-D-$(^{\alpha}\mathbf{A}^{H})_{13}$] (—), α-D-HNA + L-RNA [D-$(^{\alpha}\mathbf{A}^{H})_{13}$ + L-$(\mathbf{rU})_{13}$] (···), and L-DNA + L-RNA [L-$(\mathbf{dA})_{13}$ + L-$(\mathbf{rU})_{13}$] (—··—). All measurements were taken at 0 °C in 1 M NaCl, 20 mM KH_2PO_4, 0.1 mM EDTA (pH 7.5).

CD profiles of *ds*-α-D-HNA [*ds*-D-$(^{\alpha}\mathbf{A}^{H})_{13}$] and α-D-HNA:L-RNA [D-$(^{\alpha}\mathbf{A}^{H})_{13}$:L-$\mathbf{rU}_{13}$] confirmed the occurred formation of an heterochiral interaction. Likewise, the even larger differences between the latter and the "natural" L-DNA:L-RNA duplex (L-$\mathbf{dA}_{13}$:L-$\mathbf{rU}_{13}$) (including opposite handednesses) clearly indicated the deep structural diversity between the two structures, and therefore, differently from α-L-LNA, the limited ability by the α-L-HNA system to act as a D-DNA mimic.[35]

In a second set of experiments, the stereoselectivity of the hybridization processes of α-L-HNA was studied through annealing experiments in the mirror image world involving D-$(^{\alpha}\mathbf{A}^{H})_{13}$ and unnatural D- and L-configured complements (Table 2). As already found for similar substrates,[22,25] α-D-HNA displayed excellent hybridization capacity with β-HNA (Figure 1) and β-homoDNA (Figure 2) complements in both enantiomeric forms. Clearer than in previous studies,[25] the thermodynamic preference for the heterochiral complexes increased gradually with the sugar backbone rigidity of the oligonucleotide partners. Indeed, while in the annealing experiments between α-D-HNA and D- and L-RNA, the stability of the isochiral complex was higher than that of the corresponding heterochiral association; on the other hand, α-D-HNA formed complexes of about the same stability with the more preorganized β-D-HNA (T_m 67 °C; entry 9) and β-L-HNA (T_m 69 °C; entry 10); eventually, the stability of the complex formed between α-D-HNA and the most rigid β-L-homoDNA (T_m 58.9 °C, entry 12) was markedly higher than that of the corresponding isochiral association (T_m 50.1 °C; entry 11).

The data reported in Table 2 reveal a certain versatility in the hybridization profile of the α-HNA system. Clues on the geometry of α-D-HNA-containing associations (and reciprocally likewise on that of the corresponding α-L-HNA associations) were herein preliminarily provided by further studies of the complexes with β-D- and β-L-HNA (Figures 4−6). CD analysis

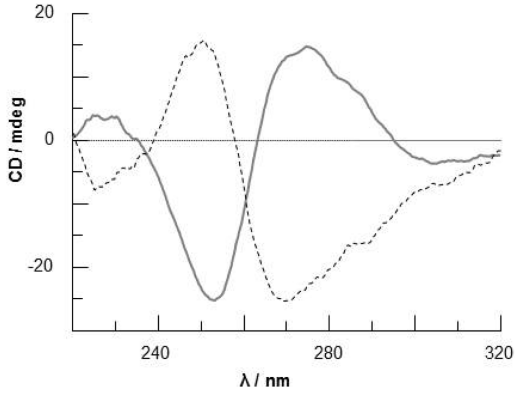

Figure 4. CD spectra of α-D-HNA + β-D-HNA [D-$(^{\alpha}\mathbf{A}^{H})_{13}$ + D-$(^{\beta}\mathbf{T}^{H})_{13}$] (—) and α-D-HNA + β-L-HNA [D-$(^{\alpha}\mathbf{A}^{H})_{13}$ + L-$(^{\beta}\mathbf{T}^{H})_{13}$] (− −). All measurements were taken at 0 °C in 0.1 M NaCl, 20 mM KH_2PO_4, 0.1 mM EDTA (pH 7.5).

surprisingly displayed that, in spite of their diastereoisomeric relationship, α-D-HNA:β-D-HNA and α-D-HNA:β-L-HNA exhibited nearly perfect mirror image profiles (Figure 4). Indeed, the CD spectrum of the α-D-HNA:β-D-HNA complex [D-$(^{\alpha}\mathbf{A}^{H})_{13}$:D-$(^{\beta}\mathbf{T}^{H})_{13}$] had a positive Cotton effect with a maximum of absorption at 275 nm and a minimum at 253 nm; conversely, the negative Cotton effect of the CD spectrum of the α-D-HNA:β-L-HNA complex [D-$(^{\alpha}\mathbf{A}^{H})_{13}$:L-$(^{\beta}\mathbf{T}^{H})_{13}$] involved a minimum of absorption at 269 nm and a maximum at 251 nm.

MD studies involving the construction of duplex models of D-$(^{\alpha}\mathbf{A}^{H})_{13}$:D-$(^{\beta}\mathbf{T}^{H})_{13}$ and D-$(^{\alpha}\mathbf{A}^{H})_{13}$:L-$(^{\beta}\mathbf{T}^{H})_{13}$ were then conducted. Early simulations aimed at the development of either quasi-linear or helical models through standard Watson−Crick base pairing gave weak and irregular structures; on the other hand, the α-D-HNA strand was found to form stable associations with β-D-HNA and β-L-HNA complements through reverse-Hoogsteen base pairing,[36] respectively appearing as smooth right- and left-handed double helices (Figure 5). Considering the high rigidity of the pyranyl sugar backbone, the formation of helical structures in both iso- and heterochiral associations is an unexpected result which has been documented only seldom before.[24] Both duplexes displayed antiparallel orientation, with a predominance for interstrand over intrastrand base stacking. As a consequence of the reverse-Hoogsteen base pairing, in both duplexes one of the grooves is

DOI: 10.1021/acs.joc.5b00406
J. Org. Chem. 2015, 80, 5014−5022

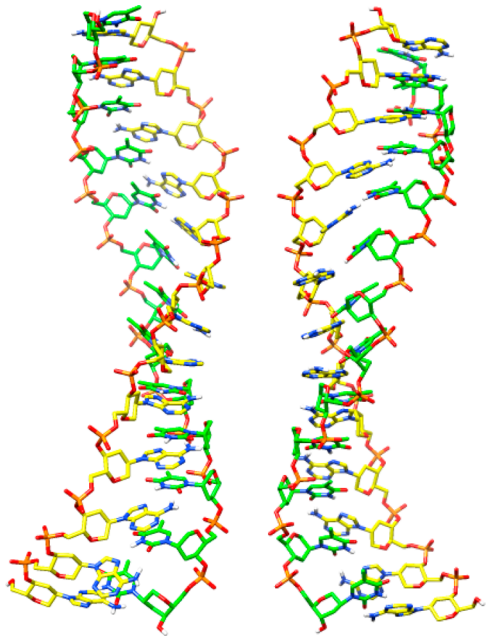

Figure 5. Left: side view of the simulated α-D-HNA:β-D-HNA duplex [D-($^{\alpha}$**A**^{H})$_{13}$:D-($^{\beta}$**T**^{H})$_{13}$]. Right: side view of the simulated α-D-HNA:β-L-HNA duplex [D-($^{\alpha}$**A**^{H})$_{13}$:L-($^{\beta}$**T**^{H})$_{13}$]. Yellow: carbon atoms in the D-($^{\alpha}$**A**^{H})$_{13}$ strand; green: carbon atoms in the D-($^{\beta}$**T**^{H})$_{13}$ and L-($^{\beta}$**T**^{H})$_{13}$ strands. Both duplexes involve reverse-Hoogsteen base pairing. In both duplexes, one of the terminal Hoogsteen base pairings is broken. Images are generated using Chimera.

hydrophobic (C8 atom of A and C5−C7 atoms in T) while the other groove (exposing N6 of A and O2 in T) is more polar.

Remarkable observations were also drawn by the analysis of the backbone torsion angles (Table 3). Both α-D-HNA and β-HNA strands exhibited α−ζ values only faintly similar to A-DNA, while they largely differed from those of B-DNA. In addition, α-D-HNA and β-D- and β-L-HNA strands displayed a much wider variability in the torsion angles than those of (A- and B-)DNA. This feature, required to enable suitable accommodation of the complementary strands regardless of their sugar chirality, is a strong indication of a certain flexibility of hexitol nucleotides within the oligonucleotide strands. A comparative analysis of the torsions in the two complexes highlighted that in the isochiral α-D-HNA:β-D-HNA duplex [D-($^{\alpha}$**A**^{H})$_{13}$:D-($^{\beta}$**T**^{H})$_{13}$] the adenine moieties of the D-*ribo*-hexitol nucleotides were arranged into unexpected *syn* conformations (average χ = −38°), while in the heterochiral α-D-HNA:β-L-HNA complex [D-($^{\alpha}$**A**^{H})$_{13}$:L-($^{\beta}$**T**^{H})$_{13}$] the same nucleotides adopted standard *anti* conformations around the glycosidic bonds (average χ = 117°). This represented the most striking difference in the conformational profile of D-($^{\alpha}$**A**^{H})$_{13}$ when involved in right- and left-handed duplexes, although other variations, especially in the backbone torsion angles α, β, and ε, also occurred (Table 3).

Larger differences in the backbone angles (especially γ, δ, ε, and ζ) were instead detected between enantiomeric β-HNA nucleotides. This was mainly the result of a sugar chair inversion[24] (^{1}C$_{4}$ → ^{4}C$_{1}$) of the L-*arabino*-hexitol nucleotides (average δ = −159°) (Figure 6b); conversely, most D-enantiomers were in the expected ^{4}C$_{1}$ form (Figure 6a), with the exception being T8, which adopts a ^{1}C$_{4}$ sugar chair (e.g., δ = 154°, very close to the value observed in the α-homoDNA:RNA duplex[38]) (Table 3). Substantially in agreement with CD analysis, despite such deep conformational differences, the two left- and right-handed duplexes overall exhibited mirror-image shapes (Figure 5), with the twist values being −18° and 22° (see the Supporting Information, Table S3).

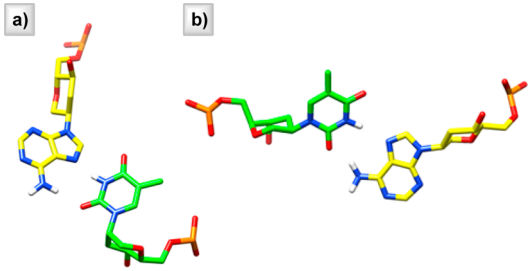

Figure 6. (a) Close-up view of the reverse-Hoogsteen base pair in D-($^{\alpha}$**A**^{H})$_{13}$:D-($^{\beta}$**T**^{H})$_{13}$. The D-*ribo*-hexitol nucleotides (yellow) adopt a ^{4}C$_{1}$ chair and a *syn* conformation around the glycosidic bond (average χ = −38°), while the D-*arabino*-hexitol nucleotides (green) adopt a ^{4}C$_{1}$ chair (axially oriented thymine; excluded T8, adopting a ^{1}C$_{4}$ chair) and an *anti* conformation around the glycosidic bond (average χ = −139°). (b) Close-up view of the reverse-Hoogsteen base pair in D-($^{\alpha}$**A**^{H})$_{13}$:L-($^{\beta}$**T**^{H})$_{13}$. The D-*ribo*-hexitol nucleotides (yellow) adopt a ^{4}C$_{1}$ chair and an *anti* conformation around the glycosidic bond (average χ = 117°), while the L-*arabino*-hexitol nucleotides (green) adopt a ^{4}C$_{1}$ chair (equatorially oriented thymine) and an *anti* conformation around the glycosidic bond (average χ = 134).

Table 3. Average Torsion Angles for Natural DNA Strands in A- and B-Form *ds*-DNA as Well as for α-D-HNA, β-D-HNA, and β-L-HNA Strands in α-D-HNA:β-D-HNA [D-($^{\alpha}$A**^{H})$_{13}$:D-($^{\beta}$**T**^{H})$_{13}$] and α-D-HNA:β-L-HNA [D-($^{\alpha}$**A**^{H})$_{13}$:L-($^{\beta}$**T**^{H})$_{13}$] Duplexes[a]**

			α-D-HNA:β-D-HNA		α-D-HNA:β-L-HNA	
	DNA (A-form)[b]	DNA (B-form)[b]	α-D-HNA	β-D-HNA	α-D-HNA	β-L-HNA
α	−*sc*	−*sc*/−*sp*	−*sc*,+*sc*	−*sc*	−*sc*	−*sc*,+*sc*
β	+*ap*	+*ac*	+*ap*/−*ap*	+*ap*/−*ap*	+*sc*,+*ac*/+*ap*[c]	+*sc*,+*ap*/−*ap*
γ	+*sc*	+*sc*	+*sc*,+*ap*	+*sc*	+*sc*,+*ap*/−*ap*	+*ap*/−*ap*
δ	+*sc*	+*ac*	+*sc*[c]	+*sc*	+*sc*	−*ap*
ε	−*ac*/−*ap*	−*ac*	+*sc*,−*ap*[c]	−*ap*	−*ap*	+*sc*/+*ac*
ζ	−*sc*	−*ap*	+*sc*,−*sc*[c]	−*sc*	−*sc*	+*sc*,+*ap*/−*ap*
χ	*anti*	*anti*	*syn*	*anti*	*anti*	*anti*

[a]The forward slash is used to indicate a continuous range in which the backbone angle values are included; the comma is used to indicate that the backbone angle values are clustered in two nonadjacent ranges. [b]Taken from ref 37. [c]A large deviation from this value was observed in T8 due to sugar chair inversion (^{4}C$_{1}$ → ^{1}C$_{4}$).

DOI: 10.1021/acs.joc.5b00406
J. Org. Chem. 2015, 80, 5014−5022

CONCLUSIONS

The synthesis and a preliminary analysis of the pairing properties of a novel member of the HNA family composed of (6′ → 4′)-linked 1′,5′-anhydro-L-*ribo*-hexitol nucleotides (α-L-HNA) have been reported through studies of a model oligoadenylate system in the mirror image world. Despite the considerable structural preorganization provided by the rigid "all equatorial" pyranyl sugar backbone, α-L-HNA (and most generally the α-HNA system) represents a truly versatile informational biopolymer, given its capability to pair with either natural or unnatural complements, regardless of the structure, conformational features, and sugar chirality of the oligonucleotide partners. This is unexpectedly the result, inter alia, of a certain degree of flexibility displayed by the nucleotide units in the oligonucleotide strand. As a case study, the iso- and heterochiral complexes deriving from the hybridization of a α-D-HNA oligoadenylate with β-HNA oligothymidylate enantiomers remarkably adopted regular, enantiomorphic double helical structures. As suggested by MD studies, the suitable accommodation of the complementary α-D-HNA and β-(D- or L-)HNA strands involved cooperative structural and conformational effects, including the unexpected formation of reverse-Hoogeteen base pairing, the *syn* nucleobase arrangement in α-D-HNA nucleotides, and the conformational change ($^1C_4 \rightarrow {}^4C_1$) of the β-L-HNA sugar units. The peculiar hybridization profile of α-(D- and L-)HNA has main relevance in the search for the structural prerequisites ruling the stereoselectivity of the hybridization processes. Herein, the observation on which the increase of the sugar core rigidity of nucleic acids (obtained replacing the natural furanose with six-membered rings) leads to a reduction in the capacity to discriminate between enantiomeric oligonucleotide partners finds in α-HNA an illustrative example. In-depth and more comprehensive studies aimed at identifying the structural factors and geometrical parameters affecting the chiral selection properties of nucleic acids are currently ongoing and will be published in due course.

EXPERIMENTAL SECTION

Nucleoside synthesis. *General.* All moisture-sensitive reactions were performed under nitrogen atmosphere by using oven-dried glassware. Solvents were dried over standard drying agents and freshly distilled prior to use. Reactions were monitored by TLC (precoated silica gel plate F254). Column chromatography: Kieselgel 60 (70−230 mesh); flash chromatography: Kieselgel 60 (230−400 mesh). ^{1}H and ^{13}C NMR spectra were recorded on NMR spectrometers operating at 200, 300, 400, or 500 MHz and 50, 75, 100, or 125 MHz, respectively. High-resolution MS analysis was performed using a quadrupole/orthogonal acceleration time-of-flight tandem mass spectrometer (qTOF2) fitted with a standard electrospray ionization (ESI) interface. Combustion analyses were performed by using a CHNS analyzer.

*4,6-Di-O-acetyl-1,5-anhydro-D-erythro-hex-2-enitol (**2**).* Iodine (69 mg, 0.27 mmol) was added to a mixture of 3,4,6-tri-*O*-acetyl-D-glucal (**1**) (3.0 g, 11.01 mmol) and Et_3SiH (5.28 mL, 33.0 mmol) in anhydrous dichloromethane (45 mL) at rt. The reaction mixture was stirred at the same temperature for 2h; then it was diluted with water and extracted with dichloromethane. The organic layers were dried (Na_2SO_4) and evaporated under reduced pressure. Chromatography of the crude residue (hexane:ethyl acetate, 100:0 to 80:20) provided the pure diacetate **2** (2.31 g, 90%). ^{1}H and ^{13}C NMR data are fully in agreement with those already reported elsewhere.[31]

*4,6-Di-O-benzyl-1,5-anhydro-D-erythro-hex-2-enitol (**4b**).* Diacetate **2** (2.3 g, 0.01 mol) was treated with a 0.1 M NaOMe solution in anhydrous MeOH (15 mL) at 0 °C. The reaction mixture was warmed to rt and stirred for 16h at the same temperature. A few drops of acetic acid were then added until neutrality, and the solvent was removed under reduced pressure. NaH (0.88 g, 0.02 mol, 60% dispersion in mineral oil) was added to a solution of crude **3** in anhydrous DMF (15 mL) at 0 °C. After 0.5h, BnBr (5.83 mL, 0.05 mol) was added in one portion to the reaction mixture. The resulting solution was warmed to rt and stirred at the same temperature for 16h. The reaction was then quenched with MeOH (3 mL), the solution was washed with aqueous NH_4Cl and extracted with AcOEt. The combined organic phases were dried (Na_2SO_4) and the volatiles removed under reduced pressure. Chromatography of the crude residue over silica gel (hexane:ethyl acetate, 100:0 to 80:20) provided the pure benzyl ether **4b** (3.08 g, 90% yield) as a colorless oil. ^{1}H NMR ($CDCl_3$, 500 MHz): δ 3.59 (ddd, *J* = 2.1, 5.5, 8.2, 1H), 3.63 (dd, *J* = 5.3, 10.3, 1H), 3.71 (dd, *J* = 2.0, 10.3, 1H), 4.04 (bd, *J* = 8.2, 1H), 4.14−4.24 (m, 2H), 4.44 (d, *J* = 11.4, 1H), 4.54 (d, *J* = 12.3, 1H), 4.59 (d, *J* = 11.4, 1H), 4.60 (d, *J* = 12.3, 1H), 5.85 (bd, *J* = 10.5, 1H), 5.92 (bd, *J* = 10.5, 1H), 7.20−7.38 (m, 10H). ^{13}C NMR ($CDCl_3$, 125 MHz): ppm 65.6, 69.5, 70.4, 71.1, 73.5, 76.3, 125.5, 127.6, 127.7, 127.9, 128.2, 128.3, 128.4, 138.1, 138.2. Elemental analysis calcd (%) for $C_{20}H_{22}O_3$: C 77.39, H 7.14; found: C 77.46, H 7.12.

*4,6-Di-O-benzyl-3-deoxy-1,5-anhydro-D-arabino-hexitol (**5b**).* THF (51 mL) was added to a stirred solution of $Hg(OAc)_2$ (4.09 g, 9.6 mmol) in H_2O (96 mL). After 15 min, a solution of olefin **4b** (3.0 g, 9.6 mmol) in THF (45 mL) was added to the reaction mixture. The resulting yellow solution was stirred for 16h at rt. Afterward, aqueous $NaBH_4$ was carefully added at 0 °C. Temperature was then raised again to rt, and the resulting gray suspension was stirred at the same temperature for 2h. The mixture was then washed with brine and extracted with AcOEt. The organic phase was dried (Na_2SO_4) and evaporated under reduced pressure. Chromatography of the crude residue over silica gel (hexane:ethyl acetate, 9:1 to 6:4) provided the pure alcohol **5b** (2.92 g, 92% yield) as a colorless oil. ^{1}H NMR ($CDCl_3$, 500 MHz): δ 1.55 (ddd, *J* = 2.8, 11.3, 13.2, 1H), 2.08 (bs, 1H, OH), 2.45 (dddd, *J* = 2.9, 3.0, 5.1, 13.2, 1H), 3.40, (ddd, *J* = 2.0, 5.4, 9.5, 1H), 3.57 (d, *J* = 12.2, 1H), 3.66 (dd, *J* = 10.5, 5.4, 1H), 3.71−3.79 (m, 2H), 3.89 (d, *J* = 12.2, 1H), 3.98 (bs, 1H), 4.38 (d, *J* = 11.4, 1H), 4.54 (d, *J* = 12.1, 1H), 4.55 (d, *J* = 11.4, 1H), 4.60 (d, *J* = 12.1, 1H), 7.18−7.36 (m, 10H). ^{13}C NMR ($CDCl_3$, 125 MHz): ppm 36.1, 66.8, 69.6, 69.9, 71.1, 72.2, 73.6, 80.7, 127.6, 127.7, 127.9, 128.3, 128.4, 138.1. Elemental analysis calcd (%) for $C_{20}H_{24}O_4$: C 73.15, H 7.37; found: C 73.09, H 7.34.

*4,6-Di-O-benzyl-3-deoxy-2-O-p-toluenesulfonyl-1,5-anhydro-D-arabino-hexitol (**7b**).* A solution of alcohol **5b** (2.4 g, 7.70 mmol) in anhydrous pyridine (65 mL) was treated with freshly purified TsCl (2.07 g, 11.0 mmol). The resulting solution was stirred at rt for 24h. The mixture was then washed with brine and extracted with AcOEt. The organic phase was dried (Na_2SO_4) and evaporated under reduced pressure. Chromatography of the crude residue over silica gel (hexane:ethyl acetate, 100:0 to 90:10) gave the pure **7b** (3.17 g, 90% yield). ^{1}H NMR ($CDCl_3$, 500 MHz): δ 1.63 (ddd, *J* = 3.0, 10.8, 13.8, 1H), 2.44 (s, 3H), 2.51 (bd, *J* = 13.8, 1H), 3.40 (ddd, *J* = 1.5, 4.4, 10.3, 1H), 3.47 (d, *J* = 13.0, 1H), 3.62 (dd, *J* = 10.7, 6.0, 1H), 3.67 (ddd, *J* = 4.4, 10.8, 10.0, 1H), 3.76 (dd, *J* = 1.5, 10.7, 1H), 3.91 (bd, *J* = 13.0, 1H), 4.33 (d, *J* = 11.3, 1H), 4.46 (d, *J* = 11.3, 1H), 4.54 (d, *J* = 12.1, 1H), 4.59 (d, *J* = 12.1, 1H), 4.76 (bs, 1H), 7.18−7.36 (m, 12H), 7.78 (d, *J* = 8.2, 2H). ^{13}C NMR ($CDCl_3$, 125 MHz): ppm 21.6, 34.2, 69.0, 69.5, 69.6, 71.4, 73.5, 77.2, 80.2, 127.6, 127.7, 127.8, 127.9, 128.3, 128.4, 129.9, 134.5, 137.8, 138.1, 144.8. Elemental analysis calcd (%) for $C_{27}H_{30}O_6S$: C 67.20, H 6.27, S 6.64; found: C 67.31, H 6.25, S 6.62.

*4′,6′-Di-O-benzyl-3′-deoxy-2′-(adenin-9-yl)-1′,5′-anhydro-D-ribo-hexitol (**8b**).* NaH (0.26 g, 66 mmol) was added to a stirring solution of adenine (1.77 g, 13.0 mmol) in anhydrous DMF (126 mL). The resulting suspension was warmed to 100 °C until a clear solution was obtained (1h). The mixture was cooled to 25 °C, then a solution of tosyl ester **7b** (3.17 g, 66 mmol) in anhydrous DMF (20 mL) was added. The solution was again warmed to 100 °C and stirred at the same temperature for 16h. The mixture was then washed with brine and extracted with AcOEt. The organic phase was dried (Na_2SO_4) and evaporated under reduced pressure. Chromatography of the crude residue over silica gel (CH_2Cl_2:MeOH, 100:0 to 95:5) provided the

DOI: 10.1021/acs.joc.5b00406
J. Org. Chem. 2015, 80, 5014−5022

pure nucleoside **8b** (1.08 g, 37% yield) as a white solid. ^{1}H and ^{13}C NMR data are identical to those already reported elsewhere.[30]

*3′-Deoxy-2′-(N^6-benzoyl-adenin-9-yl)-1′,5′-anhydro-D-ribo-hexitol (**11**).* A solution of benzyl ether **8b** (0.72 g, 1.62 mmol) in MeOH (20 mL) was purged of oxygen by bubbling nitrogen for 15 min. 10% Pd/C (0.1 g) was added and the mixture was exposed to H_2 (20 psi) while stirring for 20h. The suspension was filtered off and the filter cake was rinsed with further MeOH (4 × 25 mL). The combined filtrate was then concentrated under reduced pressure. The crude residue was dissolved in anhydrous pyridine (20 mL), the mixture was cooled to 0 °C and TMSCl (2.06 mL, 16.2 mmol) was added. After 0.5h, BzCl (0.56 mL, 4.86 mmol) was added at the same temperature. The resulting reaction mixture was warmed to room temperature and further stirred for 16h. The solution was cooled again to 0 °C, and H_2O (6 mL) and then NH_4OH (6 mL) were sequentially added. The reaction mixture was stirred at the same temperature for 1h; afterward the solvent was removed under reduced pressure. Chromatography of the crude residue (CH_2Cl_2:MeOH=90:10) afforded the pure *N*-benzoyl nucleoside **11** (0.49 g, 82% overall yield) as a white foam. ^{1}H NMR (DMSO-d_6, 400 MHz): δ 3.44−3.56 (m, 2H), 3.68−3.80 (m, 2H), 4.04 (dd, J = 3.1, 10.8 Hz, 1H), 4.56 (t, J = 5.7 Hz, 1H), 5.15 (d, J = 6.6 Hz, 1H), 7.53 (t, J = 7.3 Hz, 2H), 7.63 (t, J = 7.3 Hz, 1H), 8.02 (d, J = 7.3 Hz, 2H), 8.56 (s, 1H), 8.73 (s, 1H). ^{13}C NMR (DMSO-d_6, 100 MHz): ppm 38.0, 50.9, 61.6, 65.2, 68.7, 83.6, 126.1, 128.9, 132.9, 133.1, 133.9, 143.7, 150.8, 152.0, 152.5, 166.0. Elemental analysis calcd (%) for $C_{18}H_{19}N_5O_4$: C 58.53, H 5.18, N 18.96; found: C 58.40, H 5.20, N 19.02.

*1′,5′-Anhydro-2′-(N^6-benzoyl-adenin-9-yl)-2′,3′-dideoxy-6′-O-monomethoxytrityl-D-ribo-hexitol (**12**).* Monomethoxytrityl chloride (0.43 g, 1.40 mmol) was added at rt to a solution of diol **11** (0.43 g, 1.16 mmol) in anhydrous pyridine (18 mL) and under nitrogen atmosphere. After being stirred at the same temperature for 3h, saturated $NaHCO_3$ solution (2 mL) was added, the reaction solvent was evaporated and the resulting residue was diluted with ethyl acetate (100 mL) and washed with brine (3 × 50 mL). The organic layer was dried (Na_2SO_4), evaporated under reduced pressure and the crude residue was purified by flash chromatography (ethyl acetate) to afford the pure monomethoxytrityl ether **12** (0.63 g, 85% yield) as a white foam. ^{1}H and ^{13}C NMR data are in agreement with those already reported elsewhere.[20]

*1′,5′-Anhydro-2′-(N^6-benzoyl-adenin-9-yl)-2′,3′-dideoxy-6′-O-monomethoxytrityl-4′-O-[N,N-diisopropyl(2-cyanoethyl) phosphoramidite]-D-ribo-hexitol (**13**).* To a solution of monomethoxytrityl nucleoside **12** (0.63 g, 0.98 mmol) in anhydrous CH_2Cl_2 (6 mL), kept at 0 °C under argon atmosphere, freshly dried diisopropylethylamine (0.51 mL, 2.94 mmol) and 2-cyanoethyl-*N*,*N*-diisopropyl chlorophosphoramidite (0.33 mL, 1.47 mmol) were added. The reaction mixture was stirred at the same temperature for 2h; then saturated aqueous $NaHCO_3$ (2 mL) was added. The solution was stirred for another 10 min and partitioned between CH_2Cl_2 (50 mL) and aqueous $NaHCO_3$ (30 mL). The organic layer was washed with brine (3 × 30 mL) and the aqueous phases were back extracted with CH_2Cl_2 (30 mL). The collected organic layers were dried (Na_2SO_4) and the solvent removed under reduced pressure. Flash chromatography of the crude residue (hexane/acetone/TEA = 69/30/1) gave a foam which was dissolved in CH_2Cl_2 (3 mL) and precipitated in cold hexane (200 mL, −30 °C) containing 2% of diisopropylether, to afford the desired phosphoramidite **13** (0.74 g, 90% yield) as a white powder. The obtained product was dried under vacuum and stored overnight under nitrogen at −20 °C. Data for compound **13**: exact mass calcd for $C_{47}H_{53}N_7O_6P$ $[M + H]^+$: 842.3795, found 842.3772; ^{31}P NMR: δ 147.60, 149.01.

Oligonucleotide synthesis. Oligonucleotide assembly was performed with an Expedite DNA synthesizer by using the phosphoramidite approach. The oligomers were deprotected and cleaved from the solid support by treatment with methylamine (40% in water) and concentrated aqueous ammonia (1:1, 30 °C). After gel filtration on a NAP-10 column (Sephadex G25-DNA grade) with water as eluent, the crude mixture was analyzed by using a Mono-Q HR 5/5 anion exchange column, after which purification was achieved by using a Mono-Q HR 10/10 column with the following gradient system: A=10 mM NaOH, pH 12.0, 0.1 M NaCl; B=10 mM NaOH, pH 12.0, 0.9 M NaCl. The low-pressure liquid chromatography system consisted of a L-6200A intelligent pump, a Mono-Q HR 10/10 column, a Uvicord SII 2138 UV detector and a recorder. The product-containing fraction was desalted on a NAP-10 column and lyophilized. Oligonucleotides were purified by RPHPLC on a C-18 column prior to mass spectrometric analysis. A linear gradient of A: ammonium bicarbonate (25 mM in H_2O, pH 7.0), and B: acetonitrile (80% in H_2O) was applied.

Hybridization studies. *LC-MS analysis.* Oligonucleotides were dissolved at a concentration of 100 μM in H_2O. Samples (500 nL) were injected on a reverse phase column (C18 PepMap 0.5 × 15 mm) and eluted with a *N*,*N*-dimethylaminobutane/1,1,3,3,3-hexafluoro-2-propanol and acetonitrile system at a flow rate of 12 μL/min. Spectra were acquired using an orthogonal acceleration/time-of-flight mass spectrometer (Q-Tof-2) in negative ion mode and subsequently deconvoluted using the MaxEnt algorithm (MassLynx 3.4).

UV-melting experiments. Oligomers were dissolved in a buffer solution containing NaCl (0.1 or 1 M), potassium phosphate (0.02 M, pH 7.5), EDTA (0.1 mM). The concentration was determined by measuring the absorbance in MilliQ water at 260 nm at 80 °C and by assuming that hexitol nucleosides have the same extinction coefficients per base moiety in the denatured state as the natural nucleosides ($^{\alpha}\mathbf{A}^{H}$, e = 15000). The concentration for each strand was 4 μM in all experiments. Melting curves were determined with a spectrophotometer. Cuvettes were maintained at constant temperature by water circulation through the cuvette holder. The temperature of the solution was measured with a thermistor that was directly immersed in the cuvette. A quick heating and cooling cycle was carried out to allow proper annealing of both strands. The samples were then heated from 10 °C to 80 °C at a rate of 0.2 °C min^{-1}, and were cooled again at the same speed. Melting temperatures were determined by plotting the first derivative of the absorbance as a function of temperature; data plotted were the average of two runs. Up and down curves in general showed identical T_m values.

Circular dichroism measurements. CD spectra were measured at 5 °C with a J-715 spectropolarimeter equipped with a Peltier-type temperature control system (model PTC-348WI) in thermostatically controlled 0.1 cm cuvettes. The oligomers were dissolved and analyzed in buffer containing NaCl (0.1 or 1 M), potassium phosphate (0.2 M, pH 7.5) and EDTA (0.1 mM) and at a concentration of 8 μm of each strand.

Computational methods. *Model building and stability check of α-D-HNA-containing duplexes via molecular dynamics simulations.* MD simulations were performed for a period of 20 ns using initially AMBER 12 and later AMBER 14.[39] Atomic electrostatic charges of the HNA molecules, to be used in the Amber software package, were calculated from the electrostatic potential at the 6-31G* level using the package Gamess[40] and a RESP fitting procedure[41] (see the Supporting Information, Table S2 for the assigned atomic charges). The force field parameters used in the Amber simulations are those from the ff99bsc0 data set.[42]

Model building of duplexes. The PDB structure 2BJ6, a decameric antiparallel β-D-HNA:RNA hybrid duplex with sequence CGCG-AATTCGCG:CGCGAATTCGCG,[43] was used as a template to construct the right turning antiparallel β-D-HNA:α-D-HNA duplex [D-($^{\alpha}\mathbf{A}^{H}$)$_{13}$:D-($^{\beta}\mathbf{T}^{H}$)$_{13}$]. To "mutate" bases into Thy in the β-D-HNA strand the quatfit software from the CCL software archives was used to get the Thy base (with HNA sugar) in the right position in the duplexes (keeping sugar conformations as $^4C_1$, with Thy axially oriented). The same tool was used to add three additional Thy nucleotides to the strand to construct a 13mer strand. This single strand D-($^{\beta}\mathbf{T}^{H}$)$_{13}$ was then expanded by complementary adenine bases in a Watson−Crick configuration connected to a α-D-HNA [D-($^{\alpha}\mathbf{A}^{H}$)$_{13}$] sugar using the same tool. Those sugars have a $^4C_1$ conformation with the Ade base in an equatorial orientation.

A similar method was then tried to build the α-D-HNA:β-L-HNA duplex [D-($^{\alpha}\mathbf{A}^{H}$)$_{13}$:L-($^{\beta}\mathbf{T}^{H}$)$_{13}$]. First, L-($^{\beta}\mathbf{T}^{H}$)$_{13}$ was constructed from D-($^{\beta}\mathbf{T}^{H}$)$_{13}$ by mirroring the 3D coordinates. Starting from the right turning D-($^{\alpha}\mathbf{A}^{H}$)$_{13}$:D-($^{\beta}\mathbf{T}^{H}$)$_{13}$ duplex described above, the comple-

DOI: 10.1021/acs.joc.5b00406
J. Org. Chem. 2015, 80, 5014−5022

mentary D-($^{\beta}$**T**^{H})$_{13}$ strand was replaced by a L-($^{\beta}$**T**^{H})$_{13}$, giving us an initial antiparallel right turning heterochiral D-($^{\alpha}$**A**^{H})$_{13}$:L-($^{\beta}$**T**^{H})$_{13}$ duplex. However, preliminary force field-based calculations using Amber did not result in a stable duplex structure. Then we tried an antiparallel quasi linear duplex starting from the D-($^{\alpha}$**A**^{H})$_{13}$ single strand with angles ε = 60, ξ = −60, α = −60, β = 180, γ = 60, δ = 60 and χ (C6′C1′N9C4) = 161°. Sugars have a $^{4}C_{1}$ conformation, Ade bases being equatorially connected to the sugar. Complementary Thy bases connected to β-L-HNA sugars [χ (C6′C1′N1C2) = 112°; $^{1}C_{4}$ conformation, with the Thy bases being axially connected] were added and the final structure was fed to the leap program in the Amber suite software for energy minimization and molecular dynamics simulations.

MD simulations. Solvated molecular dynamics was used to verify the stability of the two duplexes. The structures were solvated in a truncated octahedron TIP3P water box.[44] Na^{+} counterions were added to get electrostatic neutral systems. The water molecules and counterions were then allowed to relax their positions while keeping the solute fixed. Initially, for 20 ps, the systems were heated up to 300 K with constant-T, constant-V conditions while constraining the position of the solute and using a Langevin temperature equilibration scheme. MD simulations at 300 K were initiated with periodic boundary conditions, using a cutoff distance of 10 Å for the nonbonded interactions and the particle-mesh-Ewald method for the summation of the Coulombic interactions,[45] MD time step = 0.002 ps. Total production simulation times per system were 10 ns, after an equilibration of 500 ps. Initial molecular dynamics simulations resulted in quasi-linear structures, however not very stable, resulting in irregularities in the Watson−Crick base pairing and sugar conformations. Some base pairs took a reverse Hoogsteen configuration which prompted us to force by restraints all base pairs to take this configuration. After the conformational change, the restraints were removed and the simulations were continued for 20 ns.

Analysis of the simulated structures. Clustering. The rmsd plots of the trajectories (see the Supporting Information) showed that the duplexes were very flexible. Nevertheless, the last 5 ns of the 20 ns MD trajectories were clustered into 5 groups using the average linkage algorithm implemented in the cpptraj program of the Amber software to extract a representative structure. For the different simulations, a representative structure from the cluster with the highest member count was selected.

Helical analysis. The representative structure was analyzed by a visual inspection in chimera and a curvature calculation with CURVES 5.3.[46−48] In the calculations, linearity was imposed on the axis. Because of Curves only handles Watson−Crick base pairing correctly, some of the helical parameters could not be calculated. Rise and twist were obtained from local interbase pairs and averaged over all nucleotide pairs (Supporting Information, Table S3). Images were made using the Chimera software[46] (Supporting Information, Figures S10−11).

■ ASSOCIATED CONTENT

Supporting Information

Copies of NMR spectra, MS data, UV experiments, and MD simulations. This material is available free of charge via the Internet at http://pubs.acs.org/.

■ AUTHOR INFORMATION

Corresponding Author

*E-mail: dandalonzo@unina.it.

Notes

The authors declare no competing financial interest.

■ ACKNOWLEDGMENTS

This work was supported by a FWO (Flemish Scientific Research) grant G.0784.11 and KU Leuven financial support (GOA/10/13). Mass spectrometry was made possible by the support of the Hercules Foundation of the Flemish Government (grant 20100225-7).

■ REFERENCES

(1) *Chemistry and Biology of Artificial Nucleic Acids*; Egli, M., Herdewijn, P., Eds.; Wiley-VCH: Zürich, 2012.

(2) (a) Nielsen, P. E. *Acc. Chem. Res.* **1999**, *32*, 624. (b) Lescrinier, E.; Froeyen, M.; Herdewijn, P. *Nucleic Acids Res.* **2003**, *31*, 2975. (c) Benner, S. A.; Sismour, A. M. *Nat. Rev. Genet.* **2005**, *6*, 533. (d) Hirao, I.; Kimoto, M.; Yamashige, R. *Acc. Chem. Res.* **2012**, *45*, 2055.

(3) Kaur, H.; Babu, B. R.; Maiti, S. *Chem. Rev.* **2007**, *107*, 4672.

(4) Herdewijn, P. *Chem. Biodivers.* **2010**, *7*, 1.

(5) Nielsen, P. E. *Chem. Biodivers.* **2010**, *7*, 786.

(6) Meggers, E.; Zhang, L. *Acc. Chem. Res.* **2010**, *43*, 1092.

(7) Eschenmoser, A. *Angew. Chem., Int. Ed.* **2011**, *50*, 12412.

(8) (a) Herdewijn, P.; Marlière, P. *Chem. Biodivers.* **2009**, *6*, 791. (b) Pinheiro, V. B.; Holliger, P. *Curr. Opin. Chem. Biol.* **2012**, *16*, 245.

(9) Hendrix, C.; Rosemeyer, H.; Verheggen, I.; Seela, F.; Van Aerschot, A.; Herdewijn, P. *Chem.—Eur. J.* **1997**, *3*, 110.

(10) As already reported in previous papers, the symbols "β" and "α" were used to rapidly distinguish hexitol nucleotides bearing the C2′ and C5′ substituents in a cis configuration ("β-HNA") from those displaying a *trans* relationship between the same substituents ("α-HNA").

(11) Kang, H.; Fisher, M. H.; Xu, D.; Miyamoto, Y. J.; Marchand, A.; Van Aerschot, A.; Herdewijn, P.; Juliano, R. L. *Nucleic Acids Res.* **2004**, *32*, 4411.

(12) Fisher, M.; Abramov, M.; Van Aerschot, A.; Rozenski, J.; Dixit, V.; Juliano, R. L.; Herdewijn, P. *Eur. J. Pharmacol.* **2009**, *606*, 38.

(13) Kolb, G.; Reigadas, S.; Boiziau, C.; van Aerschot, A.; Arzumanov, A.; Gait, M. J.; Herdewijn, P.; Toulmé, J.-J. *Biochemistry* **2005**, *44*, 2926.

(14) Abramov, M.; Schepers, G.; Van Aerschot, A.; Van Hummelen, P.; Herdewijn, P. *Biosensors Bioelectron.* **2008**, *23*, 1728.

(15) Kozlov, I. A.; Politis, P. K.; Pitsch, S.; Herdewijn, P.; Orgel, L. E. *J. Am. Chem. Soc.* **1999**, *121*, 1108.

(16) Vastmans, K.; Froeyen, M.; Kerremans, L.; Pochet, S.; Herdewijn, P. *Nucleic Acids Res.* **2001**, *29*, 3154.

(17) Pezo, V.; Liu, F. W.; Abramov, M.; Froeyen, M.; Herdewijn, P.; Marlière, P. *Angew. Chem., Int. Ed.* **2013**, *52*, 8139.

(18) Pinheiro, V. B.; Taylor, A. I.; Cozens, C.; Abramov, M.; Renders, M.; Zhang, S.; Chaput, J. C.; Wengel, J.; Peak-Chew, S.-Y.; McLaughlin, S. H.; Herdewijn, P.; Holliger, P. *Science* **2012**, *336*, 341.

(19) Taylor, A. I.; Pinheiro, V. B.; Smola, M. J.; Morgunov, A. S.; Peak-Chew, S.; Cozens, C.; Weeks, K. M.; Herdewijn, P.; Holliger, P. *Nature* **2015**, *518*, 427.

(20) Kerremans, L.; Schepers, G.; Rozenski, J.; Busson, R.; Van Aerschot, A.; Herdewijn, P. *Org. Lett.* **2001**, *3*, 4129.

(21) D'Alonzo, D.; Guaragna, A.; Van Aerschot, A.; Herdewijn, P.; Palumbo, G. *Tetrahedron Lett.* **2008**, *49*, 6068.

(22) D'Alonzo, D.; Van Aerschot, A.; Guaragna, A.; Palumbo, G.; Schepers, G.; Capone, S.; Rozenski, J.; Herdewijn, P. *Chem.—Eur. J.* **2009**, *15*, 10121.

(23) Krishnamurthy, R.; Pitsch, S.; Minton, M.; Miculka, C.; Windhab, N.; Eschenmoser, A. *Angew. Chem., Int. Ed. Engl.* **1996**, *35*, 1537.

(24) Froeyen, M.; Morvan, F.; Vasseur, J.-J.; Nielsen, P.; Van Aerschot, A.; Rosemeyer, H.; Herdewijn, P. *Chem. Biodivers.* **2007**, *4*, 803.

(25) D'Alonzo, D.; Amato, J.; Schepers, G.; Froeyen, M.; Van Aerschot, A.; Herdewijn, P.; Guaragna, A. *Angew. Chem., Int. Ed.* **2013**, *52*, 6662.

(26) D'Alonzo, D.; Guaragna, A.; Palumbo, G. *Chem. Biodivers.* **2011**, *8*, 373.

(27) Eschenmoser, A.; Loewenthal, E. *Chem. Soc. Rev.* **1992**, *21*, 1.

(28) Sørensen, M. D.; Kværnø, L.; Bryld, T.; Håkansson, A. E.; Verbeure, B.; Gaubert, G.; Herdewijn, P.; Wengel, J. *J. Am. Chem. Soc.* **2002**, *124*, 2164.

(29) Christensen, N. K.; Bryld, T.; Sørensen, M. D.; Arar, K.; Wengel, J.; Nielsen, P. *Chem. Commun.* **2004**, 282.

DOI: 10.1021/acs.joc.5b00406
J. Org. Chem. 2015, 80, 5014−5022

(30) Hossain, N.; Rozenski, J.; De Clercq, E.; Herdewijn, P. *J. Org. Chem.* **1997**, *62*, 2442.
(31) Yadav, J. S.; Reddy, B. V. S.; Premalatha, K.; Swamy, T. *Tetrahedron Lett.* **2005**, *46*, 2687.
(32) Bruno, T.; Borcherng, H.; Wei-Hung, C.; Yea-Fen, J.; Shuo-Cang, Z.; Subramanian, M.; Sepehr, S. *Pct. Int. Appl.* WO2005/049582 (2005).
(33) The observed regioselectivity was apparently the result of the stereoselective formation of the mercurinium ion **II** (*trans* with respect to the C5 substituent and cis with respect to the one at C4) rather than that of ion **I** (*cis* to C5 and *trans* to C4). Accordingly, it can be argued that the unfavorable interactions between the acetoxymercuric moiety and the endocyclic oxygen in **I** strongly influence the stereochemical outcome of the process; compare: (a) Paterson, I.; Smith, J. D.; Ward, R. A. *Tetrahedron* **1995**, *51*, 9413. (b) Larrosa, I.; Romea, P.; Urpi, F.; Balsells, D.; Vilarrasa, J.; Font-Bardia, M.; Solans, X. *Org. Lett.* **2002**, *4*, 4651.

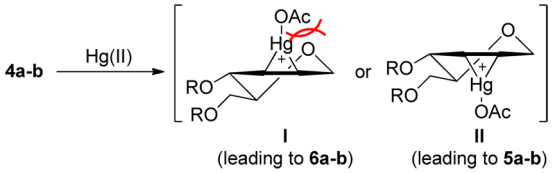

(34) As already suggested [ref 25], an uncommon kinetic control ruling the pairing process has been hypothesized to explain this phenomenon. Studies aimed to understand it are, however, underway.
(35) This last observation is not in contradiction with the overlay of Figure 2. Indeed, it is clearly established that, despite close backbone similarities of two nucleosides/nucleotides, large variations in various geometrical parameters (e.g., backbone torsion angles, helical parameters, etc.) may occur when they are incorporated into oligonucleotide strands.
(36) As widely known, a reverse-Hoogsteen A:T base pair involves hydrogen bonding between atoms N6 (A) and O2 (T) and between atoms N7 (A) and N3 (T):

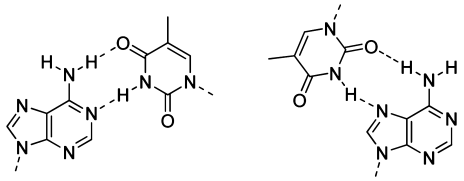

(37) Neidle, S. *Oxford Handbook of Nucleic Acid Structure*; Oxford University Press: 1999.
(38) Nauwelaerts, K.; Lescrinier, E.; Herdewijn, P. *Chem.—Eur. J.* **2007**, *13*, 90.
(39) Salomon-Ferrer, R.; Case, D. A.; Walker, R. C. *WIREs Comput. Mol. Sci.* **2013**, *3*, 198.
(40) Schmidt, M. W.; Baldridge, K. K.; Boatz, J. A.; Elbert, S. T.; Gordon, M. S.; Jensen, J. H.; Koseki, S.; Matsunaga, N.; Nguyen, K. A.; Su, S.; Windus, T. L.; Dupuis, M.; Montgomery, J. A., Jr. *J. Comput. Chem.* **1993**, *14*, 1347.
(41) Bayly, C. I.; Cieplak, P.; Cornell, W. D.; Kollman, P. A. *J. Phys. Chem.* **1993**, *97*, 10269.
(42) Perez, A.; Marchan, I.; Svozil, D.; Sponer, J.; Cheatham, T. E.; Laughton, C. A.; Orozco, M. *Biophys. J.* **2007**, *92*, 3817.
(43) Maier, T.; Przylas, I.; Strater, N.; Herdewijn, P.; Saenger, W. *J. Am. Chem. Soc.* **2005**, *127*, 2937.
(44) Jorgensen, W. L.; Chandrasekhar, J.; Madura, J.; Klein, M. L. *J. Chem. Phys.* **1983**, *79*, 926.
(45) Cheatham, T. E., III; Miller, J. L.; Fox, T.; Darden, T. A.; Kollman, P. A. *J. Am. Chem. Soc.* **1995**, *117*, 4193.
(46) Pettersen, E. F.; Goddard, T. D.; Huang, C. C.; Couch, G. S.; Greenblatt, D. M.; Meng, E. C.; Ferrin, T. E. *J. Comput. Chem.* **2004**, *25*, 1605.
(47) Lavery, R.; Sklenar, H. *J. Biomol. Struct. Dyn.* **1988**, *6*, 63.
(48) Lavery, R.; Sklenar, H. *J. Biomol. Struct. Dyn.* **1989**, *6*, 655.

DOI: 10.1021/acs.joc.5b00406
J. Org. Chem. 2015, 80, 5014−5022